The Protein Journal (2019) 38:649–657
https://doi.org/10.1007/s10930-019-09866-z

Interaction of a Model Hydrophobic Drug Dimethylcurcumin with Albumin Nanoparticles

R. P. Das[1,2] · B. G. Singh[1,2] · A. Kunwar[1,2] · K. I. Priyadarsini[2,3]

Published online: 6 September 2019

Abstract
The aim of present study was to investigate the binding interactions of a model hydrophobic molecule, dimethylcurcumin (DMC) with nanoparticle form of bovine serum albumin (BSA) using fluorescence spectroscopy techniques. For this, BSA nanoparticles (size = 62.0 ± 3.5 nm, molecular weight = 11,243 ± 3445 kD) prepared by thermal denaturation method was mixed with DMC in solution and monitored for fluorescence emission of tryptophan (Trp) residue as well as DMC separately. The emission maximum of DMC in nanoparticles form exhibited more blue sift and quenched the excited state of tryptophan (Trp) by six fold higher than in the native form of BSA. By analyzing Trp fluorescence, the mean binding constant (K) estimated for the interaction of DMC with native and nanoparticles forms of BSA was $2.7 \pm 0.4 \times 10^4$ M^{-1} and $1.5 \pm 0.5 \times 10^5$ M^{-1} respectively. Together these results suggested that DMC experienced a more rigid environment in nanoparticles than in native form of BSA. Additionally the above determined K values were in agreement with those reported previously by absorption techniques. Further direct energy transfer was observed between Trp and DMC, using which the distance (r) calculated between them was 28.25 ± 0.27 Å in BSA native. Similar analysis involving BSA nanoparticle and DMC revealed a distance of 24.25 ± 1.05 Å between the hydrophobic core and the ligand. Finally interaction of DMC with BSA was validated through molecular docking studies, which indicated sub-domain IIA as the binding site of DMC. Thus it is concluded that intrinsic fluorescence of protein can be utilized to study the interaction of its different physical forms with any hydrophobic ligand.

Keywords Albumin · Nanoparticles · Fluorescence spectroscopy · Binding constant · Fluorescence energy transfer

1 Introduction

In recent times, proteins have emerged as the material or excipient of choice for developing formulations of nutraceutical and pharmaceutical applications [1–4]. Proteins as an excipient offer several advantages like biodegradability, biocompatibility and possibility of interaction with a wide range of bioactive or pharmacologically important molecules [3–5]. Serum albumin is one such class of protein which is studied extensively as carriers for drug and food grade molecules [6–8]. Albumin is the major soluble protein of the circulatory system of vertebrates comprising about 60% of the total protein content of plasma. It is involved in the transport of nutrients to cells, regulation of plasma buffer and maintenance of osmotic pressure [6–8]. With the advent of nanotechnology, there has also been a lot of interest in exploring albumin nanoparticles as novel drug delivery system [9, 10]. Indeed there is a commercial grade formulation, Abraxane® available in the market which constitutes human

Electronic supplementary material The online version of this article (https://doi.org/10.1007/s10930-019-09866-z) contains supplementary material, which is available to authorized users.

✉ B. G. Singh
beenam@barc.gov.in

✉ A. Kunwar
kamit@barc.gov.in

[1] Radiation & Photochemistry Division, Bhabha Atomic Research Centre, Trombay, Mumbai 400085, India

[2] Homi Bhabha National Institute, Anushaktinagar, Mumbai 400 094, India

[3] Chemistry Division, Bhabha Atomic Research Centre, Trombay, Mumbai 400085, India

serum albumin nanoparticles-bound paclitaxel [11]. The principle behind the formation of albumin nanoparticles is the aggregation of denatured protein molecules to form stable nuclei, which subsequently serves as seeds for nanoparticle growth [2, 4, 5, 12]. Some of the common methods of preparing albumin nanoparticles are the simple precipitation using anti-solvent and the thermal or chemical denaturation followed by precipitation [13, 14]. The later methodologies have advantage over the simple precipitation of generating stable particles, which are not disintegrated under physiological conditions [14]. The efficiency of an albumin based nano-formulation for encapsulation and controlled release depends mainly on its mode of interaction and binding strength with ligand molecules [14, 15]. Therefore understanding the molecular insight of ligand–protein interaction would greatly advance the rational development of economically successful food and/or pharmaceutical formulations.

Although a number of spectroscopic techniques including UV–Visible spectroscopy is available for the study of interaction between protein and various drug molecules, the one employing fluorescence is simple and very sensitive method for studying the same [16]. In general fluorescent moieties (fluorophores) absorb light of a specific wavelength (λ_{ex}), and after a brief interval, termed the fluorescence lifetime (τ), energy is emitted at a longer wavelength (λ_{ex}) [16, 17]. However, this approach may require fluorescent labeling. Such labeling may not always be possible or even desirable since attaching a fluorescent dye to a bio-molecule may partially alter its physical and chemical properties. On contrary many proteins contain naturally fluorescent amino acids, such as tryptophan (Trp) and tyrosine (Tyr) [16, 17]. Accordingly a large number of reports have established that the intrinsic Trp fluorescence in proteins can be effectively used to study the drug-protein interaction [8, 18]. Dimethyl curcumin (DMC) is one such pharmacologically important model hydrophobic molecule. It is the metabolically stable derivative of curcumin, a polyphenol from rhizome of *Curcuma longa* [19, 20]. It is known to possess diverse pharmacological activities and also exhibits solvent dependent photo-physical properties [21]. Recently our group has studied its interaction with different physical forms of BSA using UV–Visible spectroscopy [14]. In continuation to this work, here in the present study, fluorescence spectroscopic techniques were optimized to investigate the same and the results were compared with those reported previously. For this, BSA nanoparticles of ~60 nm size prepared employing a previously optimized thermal denaturation method was used [14]. The native and nanoparticle forms of BSA were compared for the fluorescence intensity, emission maximum (λ_{max}), anisotropy and fluorescence life time of intrinsic Trp residues to understand the changes in molecular environment during nanoparticles formation. Next, quenching of Trp fluorescence in native and nanoparticles forms of BSA by DMC was studied in detail to determine binding parameters. Since fluorescence resonance energy transfer (FRET) can occur between Trp and DMC with the latter one as the final acceptor molecule, this tool was employed to map the location of DMC in the microenvironment of native and nanoparticles forms of BSA. Finally docking studies were performed to validate the interaction of DMC with BSA.

2 Methods and Materials

2.1 Chemicals

BSA, sodium hydrogen phosphate (monobasic and dibasic), potassium hydrogen phosphate, sodium chloride and potassium chloride from Sigma chemicals were purchased through local agents. Dimethyl curcumin (DMC) with 99% purity was obtained as a kind gift from M/s. Nastol Laboratories, Vishakhapatanam. The synthesis and characterization of DMC is mentioned in previous report [21]. The solvents like dimethyl sulfoxide (DMSO), ethanol and methanol were procured from Sisco Research Laboratories (Mumbai, Maharashtra). Dialysis membrane-60 of diameter 15.9 mm and molecular cutoff 12-14 kDa was purchased from Himedia. Solutions were prepared in nano pure water from a Millipore Milli-Q system. All other chemicals with maximum available purity were purchased from reputed local manufacturers/suppliers.

2.2 Preparation of BSA Nanoparticles

For this 150 µM (1% w/v) of BSA solution in phosphate buffer saline (PBS) was processed by thermal denaturation (68 °C) method as described in our previous report to obtain spherical shaped BSA nanoparticles of mean hydrodynamic diameter of 62.0 ± 3.5 nm (polydispersity index of 0.175) with a corresponding zeta (ζ) potential value of -6.0 ± 0.29 mV (Figs. S1 and S2A) [14]. Further high pressure size exclusion chromatography (HP-SEC) was performed using AKTA purifier (GE Healthcare, USA) to determine the molecular weight of BSA nanoparticles [22]. The column (Superose 6 increase 10/300 GL) was pre-equilibrated with buffer (PBS, pH 7.5) at a flow rate of 0.5 ml/min. Around 100 µl aliquot of nanoparticle sample equivalent to a protein concentration of 10 µg/µl was injected and the eluted protein was detected by following absorbance at 280 nm.

2.3 Photophysical Studies

A freshly prepared DMC solution (2.7 mM or 1 mg in 1 ml) in ethanol and 150 µM (1% w/v) of BSA native or nanoparticles in PBS was used for fluorescence titration

and estimation of the binding constant. In brief the above two solutions were mixed very quickly to obtain the required concentration of BSA and DMC in a reaction system of 3 ml and subjected to fluorescence measurement. The ethanol content in the reaction mixture did not exceed 1%. The steady-state fluorescence measurements were carried out in a quartz cuvette (1 cm × 1 cm) using a Hitachi spectro-fluorimeter (model F-4500; Tokyo, Japan) with a slit width of 2.5 nm for the excitation and emission beams. Fluorescence anisotropy values were calculated using parallel and perpendicular polarizers according to equation mentioned below:

$$\text{Anisotropy (r)} = \frac{(I_{vv} - GI_{vh})}{(I_{vv} + 2GI_{vh})} \quad (1)$$

where I_{VV} and I_{VH} are the fluorescence intensities determined at vertical and horizontal orientations of the emission polarizer, respectively, when the excitation polarizer is set in the vertical position. The G factor, which compensates for differences in the detection efficiency for vertically and horizontally polarized light, was calculated from the fluorescence intensity ratio of vertical and horizontal emissions when the excitation polarizers set in the horizontal position (I_{HV}/I_{HH}) [23, 24].

Fluorescence life times were measured using a time-correlated single photon counting (TCSPC) spectrometer (Horiba Jobin Y von, UK). The samples were excited by light pulses from a nano-LED source (292 nm, repetition rate of 1 MHz) and the fluorescence was detected using a PMT based detection module (model TBX4). A reconvolution procedure was used to analyze the observed decays using a proper instrument response function obtained by substituting the sample cell with a light scatterer (turbid solution of TiO_2 nanoparticles in water). With the present setup, the instrument time resolution is adjudged to be about 40 ps. The fluorescence decays were analyzed as a sum of exponentials as,

$$I(t) = \sum_i B_i \exp(-t/\tau_i) \quad (2)$$

where I (t) is the time-dependent fluorescence intensity and B_i and τ_i are the pre-exponential factor and the fluorescence lifetime for the ith component of the fluorescence decay, respectively. The quality of the fits and consequently the mono/multi-exponential natures of the decays were judged by the reduced Chi square (χ^2) values and the distribution of the weighted residuals among the data channels. For a good fit, the χ^2 value was close to unity and the weighted residuals were distributed randomly among the data channels [25, 26].

2.4 Preparation of BSA-DMC Complex for FRET

To prepare BSA-DMC complex, 5 µl of DMC stock solution (50 mg/ml in DMSO) was mixed with 2 ml of 1% (w/v) BSA native or nanoparticles solution, stirred for 20 min and dialyzed to remove the unbound DMC and DMSO using PBS as dialyzing solvent for 24 h under constant stirring at 100 rpm. The concentration of DMC in the purified BSA native and nanoparticles solution was determined as 250 µM and 300 µM respectively by employing UV–Visible absorption technique (at 420 nm) as reported previously. The above prepared BSA-DMC complex was appropriately diluted using blank BSA native or nanoparticles and used for FRET as well as fluorescence microscopy.

2.5 Molecular Docking

The optimized structure of the DMC was docked on BSA (obtained from protein data bank,) using Lead IT 2.1.3-FlexX (BioSolve IT, GmbH, Germany) docking software. The structure of DMC was optimized using density functional theory (DFT) method and B3LYP/6-31 + G(d,p) level of GAMESS software in gaseous state and saved as Mol2 file. The crystal structure of BSA protein was downloaded from protein data bank (PDB file: 3V03). The protein was loaded into LeadIT 2.1.2 and the receptor components were chosen by selection of chain A as a main chain without any reference ligand. Binding site was defined by choosing amino acid residues present in the given domains. Amino acids within radius 10 Å were selected in the binding site. Ligand binding was checked by using enthalpy (classic Triangle matching), entropy (single interaction scan) and the hybrid method (which utilizes both enthalpy and entropy based binding). For scoring, all default settings were restored. Intra-ligand clashes were computed by using clash factor of 0.6. The base placement method was used as a docking strategy [27].

3 Results

3.1 Determination of Molecular Weight and Aggregation Number of BSA Nanoparticles

The molecular weight of BSA nanoparticles was determined by HP-SEC. The elusion profiles presented in Fig. 1 showed the appearance of a single major peak at approx. 33 min and a broad distribution ranging from 17 to 20 min in case of BSA native and nanoparticles forms respectively. The broad distribution is attributed to the polydispersity of nanoparticles. The calibration curve of retention time verses molecular weight was prepared using standard proteins such as carbonic anhydrase (29 kDa), BSA (66 kDa), alcohol

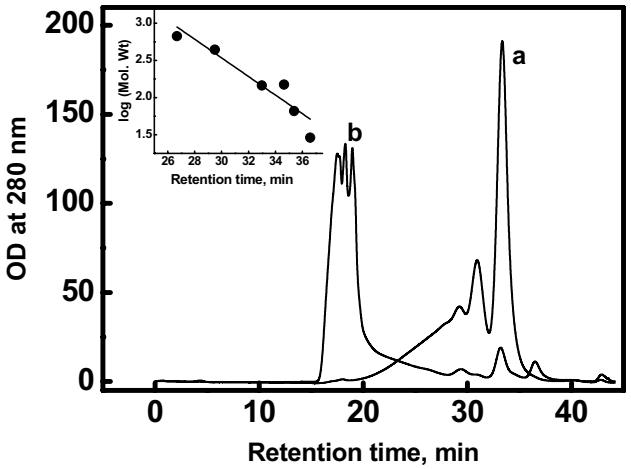

Fig. 1 Chromatograms of BSA solution in its (*a*) native and (*b*) nanoparticles form. Inset shows the calibration plot of retention time obtained with standard proteins of known molecular weights

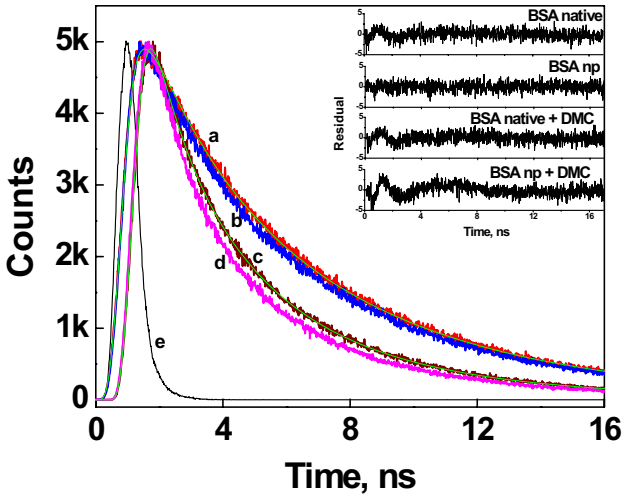

Fig. 2 Fluorescence decay curve along with the biexponential fitted curve (smooth line) shows the decay of Trp emission at 340 nm after excitation at 292 nm. Inset shows the distribution of the residuals. The decay trace (*a*) and (*b*) corresponds to Trp in 30 μM BSA native in absence and presence of 40 μM DMC, respectively. Similarly, the decay trace (*c*) and (*d*) corresponds to the decay of Trp in 30 μM BSA nanoparticles in absence and presence of 40 μM DMC. The instrument response function is given in plot (e)

dehydrogenase (150 kDa), amylase (200 kDa), apoferritin (443 kDa) and thyroglobulin (669 kDa) (inset of Fig. 1). Using this calibration curve, the estimated average molecular weight of BSA nanoparticles was 11,243 ± 3445 kDa. Further by taking the ratio of the molecular weights of nanoparticles and native forms, the number estimated of BSA monomers comprising a single nanoparticle was 170 ± 52. Notably, our group had previously reported that BSA nanoparticles of ~ 60 nm synthesized by thermal denaturation method was composed of 466 number of BSA monomers [14]. The higher aggregation number obtained in previous study could be due to fact that it was calculated taking into account of the hydrodynamic size of the native and nanoparticles. Since the aggregation number reported in present study is based on the actual mass values, it appears to be a more accurate way of representing BSA nanoparticles.

3.2 Fluorescence Lifetime and Anisotropy of Trp During the Formation of BSA Nanoparticles

The fluorescence (λ_{max} = 340 nm) of BSA protein upon excitation at 292 nm is attributed to Trp213 residue embedded in the hydrophobic pocket of sub-domain IB [14]. The emission maximum and fluorescence life time of Trp are highly sensitive to environment polarity and thus are expected to predict the conformational changes during the formation of BSA nanoparticles from its native form [4, 14, 28]. Our group has previously shown that emission maximum of BSA in the nanoparticle form is slightly blue sifted to 335 nm as compared to 340 nm of native form [14]. This clearly suggested that most of the Trp residues in BSA nanoparticles are less exposed to solvent compared to native form and thus are expected to be deeply buried inside the hydrophobic core formed during the aggregation or nucleation process of nanoparticles growth [4, 28]. In this study to determine the fluorescence life time of Trp, 30 μM of BSA in native and nanoparticle form was excited at 292 nm and the emission intensity was collected at 340 nm as a function of time. The fluorescence decay profile (Fig. 2) of BSA native could be fitted to biexponential function with relative fluorescence lifetimes of 2.80 ns (17%) and 6.42 ns (83%) and average life time of 5.82 ns (τ_o). Similarly in nanoparticles form, the temporal fluorescence profile showed biexponential decay, with relative fluorescence lifetimes of 1.99 ns (37%) and 5.35 ns (63%) and average lifetime of 4.16 ns (Fig. 2). Our value on the fluorescence lifetime of Trp in BSA native is in agreement with literature reports [29]. The decrease in average fluorescence life time of Trp during the formation of BSA nanoparticles may be due to energy transfer or some other competing photophysical processes with neighboring amino acids brought in close vicinity by aggregation/nucleation process. This assumption is supported by some recent reports indicating that the aggregation of protein monomers leads to the decrease in fluorescence life time of intrinsic Trp residue [30, 31]. Further steady-state fluorescence anisotropy measurement of BSA in different physical forms can disclose the extent of rotational freedom and dynamics available to the Trp side chain in the excited state. Accordingly fluorescence anisotropy of Trp residue in the native and nanoparticles forms of BSA was monitored by collecting emission from 300 nm to 400 nm after excitation at 290 nm. The results presented in Fig. S3 indicated that there was no significant change in the

anisotropy of Trp in the native and nanoparticle forms of BSA. This clearly suggested that the aggregation of BSA monomers during the formation of nanoparticles although led to minor change in local environment did not impose any additional restriction on the rotational mobility of Trp side chain.

3.3 Estimation of the Binding Parameters of DMC with BSA Native/Nanoparticles Using Trp Quenching

In order to estimate the binding parameters of DMC with BSA native or nanoparticles, fluorescence titration experiment was performed by varying the concentration of DMC from 1 to 10 µM and keeping the concentration of protein (BSA native or nanoparticle) fixed at 30 µM. The above concentration of DMC was chosen, so that its absorbance at 290 nm did not increase by more than 10% of the absorbance of the macromolecule. The reaction mixture was monitored for Trp fluorescence at 340 nm after excitation at 290 nm. It was observed that the fluorescence intensity due to Trp in both native as well as nano-particle forms decreased/quenched in the presence of DMC (Fig. 3). This confirmed the binding of DMC with BSA native and its nanoparticle form. The change in fluorescence intensity was analyzed to estimate the binding constant according to Eq. (3).

$$\log \frac{(F_0 - F)}{F} = \log K + n \log [DMC] \tag{3}$$

here F_o and F are the corrected fluorescence intensity for inner filter effect from Trp, at 340 nm in the absence and the presence of different concentrations of DMC. K is the binding constant of DMC with the macromolecule in its native and nanoparticles form and n is the number of DMC molecule bound to the macromolecule. The slope and intercept of the linear fit of the double logarithmic plot as presented in the inset of Fig. 3 was used to calculate the binding parameters n and K and these values were 1.01 ± 0.16 and $2.63 \pm 0.36 \times 10^4$ M^{-1} respectively for BSA native and 1.13 ± 0.21 and $1.55 \pm 0.53 \times 10^5$ M^{-1} respectively for BSA nanoparticles. Further the binding of DMC to BSA native or nanoparticle is also expected to affect the fluorescence life time of Trp. To verify this, fluorescence lifetime of Trp was measured by varying the concentration of DMC from 5 to 40 µM and keeping the concentration of protein (BSA native or nanoparticle) fixed at 30 µM. The results indicated that average fluorescence life time of Trp in both native and nanoparticles forms successively decreased with the increasing concentration of DMC (Fig. 4). The fluorescence quenching constant was determined by employing Stern–Volmer Eq. (4).

$$(\tau_0/\tau) - 1 = k_q \tau_0 [DMC] \tag{4}$$

where τ_0 and τ are the excited state lifetime of Trp in the absence and presence of DMC, respectively and k_q is the fluorescence quenching constant. The estimated k_q value for native and nanoparticle form was $1.37 \pm 0.04 \times 10^{13}$ M^{-1}/s and $4.40 \pm 0.03 \times 10^{13}$ M^{-1}/s respectively. Higher quenching constant in BSA nanoparticle form indicates that DMC is located in close vicinity to fluorescent Trp moiety.

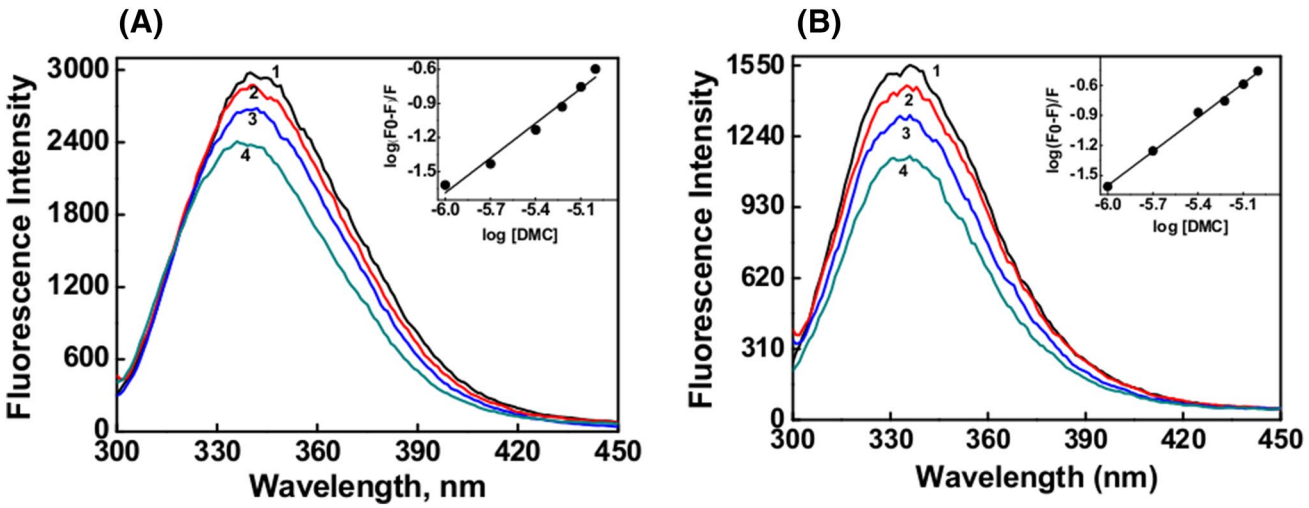

Fig. 3 Fluorescence spectra of aqueous solutions containing 30 µM BSA native (graph **A**) and BSA nanoparticles (graph **B**) with varying concentration of DMC from 1 µM to 10 µM at pH 7.4. Spectra 1–4 corresponds to 0, 2, 6 and 10 µM DMC. Inset of the figures shows the double logarithm plot of tryptophan fluorescence against DMC concentration

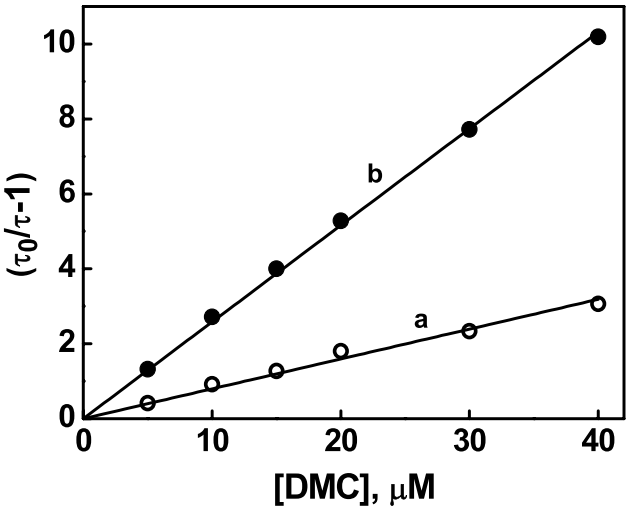

Fig. 4 Stern–Volmer quenching plot of (*a*) BSA native and (*b*) BSA nanoparticle by varying concentration of DMC (5–40 μM) at pH 7

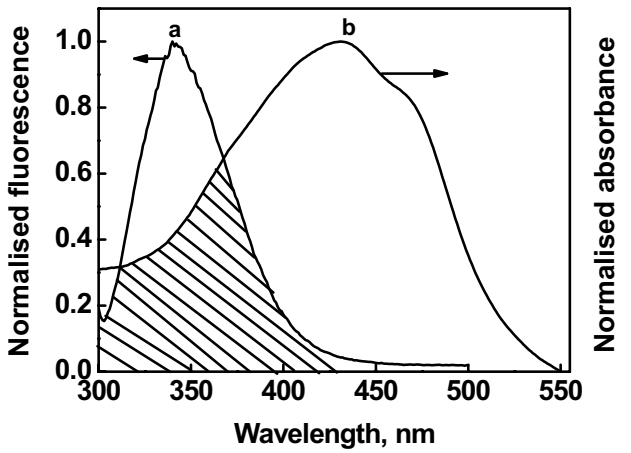

Fig. 5 Spectra showing overlap between the fluorescence spectrum of BSA (spectrum a) and the absorption spectrum of DMC (spectrum b). The overlap integral *J* is calculated according to (8)

3.4 FRET Studies of BSA-DMC Complex

The emission spectrum of Trp in BSA native or nanoparticle overlaps with the absorption spectrum of DMC (Fig. 5) [14]. This pointed out that the quenching of Trp or the decrease in its life time in presence of DMC might be due to the energy transfer from the excited state of Trp to the ground state of DMC. To address this, 30 μM of DMC bound to 30 μM of BSA (native or nanoparticle) was prepared by dialysis as mentioned in the experimental section. The BSA-DMC complex was excited at 290 nm and monitored for DMC emission spectrum from 450 to 650 nm. A cut-off filter of 420 nm was used to avoid the interference from Trp emission. As seen from Fig. S4, the emission of DMC was observed on excitation of Trp at 290 nm. This energy transfer is a non-radiative mode, and can be utilized to estimate the distance between the Trp and DMC using Förster's theory of resonance energy transfer [17, 28]. As explained earlier, unlike to native form, the fluorescence emission of BSA nanoparticles is attributed to several Trp residues buried in its hydrophobic core. Accordingly FRET analysis in BSA nanoparticle is expected to indicate the distance between DMC binding site and its fluorescent hydrophobic moiety. The efficiency of energy transfer (*E*) is related to the distance *r* (Å) between the donor and acceptor by Eqs. (5 and 6),

$$E = \frac{R_o^6}{R_o^6 + r^6} = 1 - \frac{\tau}{\tau_o} \tag{5}$$

$$k_{et} = \frac{1}{\tau_0}\left(\frac{R_0}{r}\right)^6 \tag{6}$$

In the above equation $R_o$is defined as critical transfer distance at which the transfer efficiency equals 50% or the fluorescence of donor is quenched by 50%. R_o can be calculated by using the following relation,

$$R_o = 9.79 \times 10^3 \left(\kappa^2 \Phi_o J \eta^{-4}\right)^{1/6} \text{Å} \tag{7}$$

where *J* is the spectral overlap integral between the donor emission and the acceptor absorption, and κ^2 is the orientation factor between the emission of the dipole of the donor and the absorption dipole of the acceptor, which is generally 2/3 for isotropic donor and acceptor, Φ_0 is the quantum yield of the donor i.e. Trp and η is the refractive index of the medium. Using pure Trp as reference solute, the Φ of Trp in BSA native and nanoparticle was estimated by relative method [28] and found to be 0.10 and 0.07, respectively (experimental uncertainty = 5%). The spectral overlap integral (*J*) between the donor emission spectrum and the acceptor absorption spectrum was determined by,

$$J(\lambda) = \left(\int_0^\infty F_D \varepsilon_A \lambda^4 d\lambda\right) \Big/ \left(\int_0^\infty F_D d\lambda\right) \tag{8}$$

here F_D and ε_A represent the fluorescence intensity of the donor and the molar extinction coefficient of the acceptor respectively at the wavelength λ. Spectral overlap integral J value estimated was 9.52×10^{-15} M^{-1} cm^3 and 1.13×10^{-14} M^{-1} cm^3 for the complex of DMC bound with BSA native and nanoparticle, respectively. Using the above parameters and according to Eq. (7), the value of R_o

estimated was 23.1 Å and 23.8 Å for native and nanoparticle form, respectively.

The efficiency (E) of energy transfer for BSA native and nanoparticle forms was determined using respective fluorescence life time τ_0 and τ in the absence and presence of DMC. Further by applying R_o value into Eqs. (5 and 6), k_{et} and the distance(r) between the DMC binding site and Trp 213 in BSA native was estimated to be $0.52 \pm 0.03 \times 10^8$ s^{-1} and 28.25 ± 0.27 Å respectively. Similarly, k_{et} and the distance (r) between the DMC binding site and fluorescence moiety (Trp) in BSA nanoparticle was estimated to be $2.16 \pm 0.21 \times 10^8$ s^{-1} and 24.25 ± 1.05 Å respectively.

3.5 Steady State Fluorescence Anisotropy Measurement of DMC Upon Binding with BSA Native or Nanoparticle

DMC has previously been reported to exhibit solvent sensitive emission maximum and with decrease in solvent polarity, the emission maximum of DMC displays a marked blue shift [14, 32]. For example emission maximum of DMC in water (~550 nm) is significantly blue shifted when bound to BSA in its native state (~510 nm) and nanoparticles form (500 nm) (Fig. S5) [14]. Also, binding of DMC with BSA in its native and nanoparticle form, resulted in increase in the emission intensity by 3 and 7 times, respectively, indicating increase in the emission quantum yield of DMC in BSA nanoparticles as compared to native form (Fig. S6). Thus the fluorescence enhancement and blue shift in emission maximum of DMC bound to BSA suggested that the local polarity of DMC at the binding site of BSA is very much lower than that in bulk water. Additionally it can be inferred that DMC is located in a relatively rigid environment resulting in decrease in the non-radiative process. To further validate this, anisotropy of DMC (10 µM) bound to 30 µM of BSA native or nanoparticles was investigated by exciting at 420 nm (absorption maximum of DMC) and monitoring the emission from 440 nm to 630 nm. The anisotropy of DMC significantly increased from 0.02 in aqueous methanol solution to ~0.35 in the presence of BSA native or nanoparticles (Fig. 6). This confirmed that the motion of DMC was restricted upon binding to BSA native or nanoparticles causing an increase in the steady-state anisotropy. However, because of very short fluorescence life time of DMC, its rotational dynamics could not be attempted.

Having understood the changes in fluorescence emission of DMC on its interaction with BSA native or nanoparticles, the binding studies were also performed by monitoring the fluorescence of DMC after excitation at 420 nm. For this the concentration of DMC was varied from 1 to 10 µM and the concentration of protein (BSA native or nanoparticle) was fixed at 30 µM. The emission intensity obtained at 510 nm (Fig. S6) was used to estimate the K values using Eq. No (4).

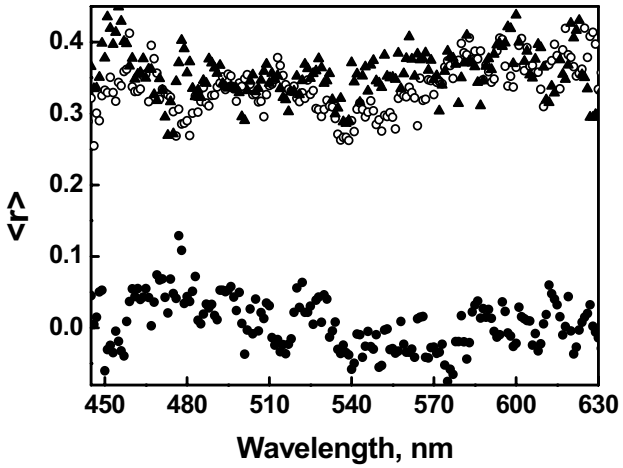

Fig. 6 Steady-state fluorescence anisotropy of aqueous solutions of 10 mM DMC in (filled circle) PBS solution, (open circle) BSA native and (filled triangle) BSA nanoparticle at pH 7

$$I_f = \frac{I_o + I_{\max} K[DMC]}{1 + K[DMC]} \quad (6)$$

where I_o and I_{max} are the corrected emission intensities of DMC in absence and presence of the macromolecule respectively. Using the non-linear equation, the respective K value for BSA native and BSA nanoparticle was estimated to be $6.1 \pm 0.4 \times 10^3$ M^{-1} and $1.2 \pm 0.1 \times 10^4$ M^{-1}. To further validate the binding of DMC with BSA nanoparticle, fluorescence imaging was performed. For this, the solution of DMC (10 µM)–BSA (30 µM) nanoparticle was air dried on a glass cover slip and fluorescence images were captured after excitation with blue filter (450–480 nm). The images presented in Fig. S2B showed a very bright fluorescence from spherical dots confirming the binding of DMC with BSA nanoparticle.

3.6 Molecular Docking

DMC has a α,β-diketo unsaturated moiety which can exhibit keto-enol tautomerism. The ground state optimized structure of both the keto and enol form indicated that the enol form is more stable by −4 kcal/mol. The optimized structure of DMC in the enol form was used for docking on native BSA. As the PDB file of the BSA nanoparticle was not available, the docking studies could not be performed for the nanoparticle form. The docking was executed by exploring initially the enthalpy and the entropy mode of interaction separately and then using both the modes simultaneously with the help of the in-built program in the Lead IT software. The favored binding site of DMC on BSA native was evaluated on the basis of free energy change as obtained from the HYDE algorithm of the Lead IT software. The most stable binding

of DMC was found to be in domain IIA of BSA native with entropy mode (single scan interaction) giving the most stable pose with free energy value of − 30 kJ/mol. The free energy change on binding of DMC with IIA domain as estimated by employing triangle matching and the hybrid approach was − 10 kJ/mol. Thus the docking studies also supports that the interaction of BSA native form with DMC is mostly by hydropobic interaction. Figure 7 shows the representative pose of DMC in IIA domain of BSA native form, which is calculated by entropy mode. It can be seen that Glu (glutamate) 229 and 226 are involved in electrostatic interaction via their amine group with the enol form of DMC. Further these residue along with Lys 224, 232, Asp268, Val228, Thr269 are involved in hydrophobic interaction (as seen by green lines) with the aromatic moiety of DMC. The pose view of DMC bound to BSA native by enthalpy mode is presented in Fig. S7.

4 Discussion

The physiological role of albumin as a transport protein along with its increasing importance in pharmaceutical, nutraceutical and food industries has generated a lot of interest among researcher to understand its interaction with biologically relevant molecules [6–8]. The most important parameter that defines the strength of interaction of a ligand with albumin protein is the equilibrium or binding constant (K) value [6–8]. The K of ligand varies depending on the physical forms of albumin protein. In general

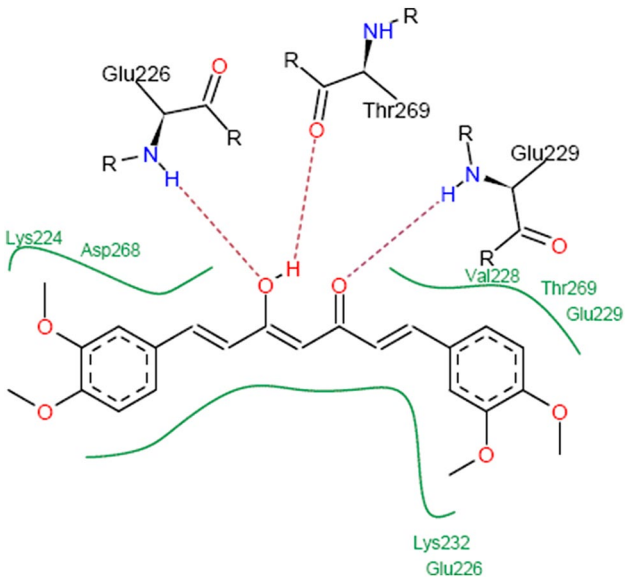

Fig. 7 Schematic representation of the amino acids involved in binding of DMC with BSA native in domain IIA by entropy mode. Here, green line represents hydrophobic site of interaction, whereas the dotted line represents the electrostatic interaction

protein nanoparticles formed due to aggregation of denatured monomers show higher K and entrapment efficiency for hydrophobic ligands facilitating better solubility, stability and bio-distribution [3, 9–11, 14]. This observation has led to the emergence of protein nanoparticles as a novel excipient [33]. Drug-protein interactions can be investigated by various methods like FT-IR, circular dichroism, etc. However fluorescence technique is more sensitive and informative as it utilizes the changes in the micro-environment of protein as well as ligand. The present manuscript demonstrates that owing to intrinsic fluorescence of Trp residue present in BSA native or nanoparticles, fluorescence technique serves as a sensitive tool to study their interaction with a hydrophobic molecule like DMC. Our results clearly support that fluorescence emission maximum and life time of Trp residue in albumin protein is highly sensitive to any change in its physical form or the binding of a hydrophobic ligand. These changes can be conveniently employed to calculate the K value and to understand the molecular process involved in the interaction. For example as expected DMC showed higher K with nanoparticles of BSA than with its native form. The higher binding strength of DMC with BSA nanoparticle may be attributed to the difference in the polarity of its inner core compared to that of native form [4, 14]. The inner core of nanoparticle is expected to be more hydrophobic in nature [4, 14]. Indeed our results showing a blue shift in the emission maximum along with decrease in fluorescence life time of Trp in BSA nanoparticle confirmed above assumption. Notably K value obtained by fluorescence method matches with that reported previously using UV–Visible spectroscopy [14]. This validates the utility of fluorescence techniques for binding studies. Like Trp fluorescence of albumin protein, the inherent fluorescence property of the ligand can also be utilized to study the drug-protein interaction [34]. DMC upon binding to native or nanoparticles forms of BSA showed blue shift in its emission maximum [14]. By comparing the emission maximum of DMC in BSA native and nanoparticles with those of different polarity solvents, it was predicted that DMC in the BSA native and BSA nanoparticle was present in an environment having dielectric constant of 37.5 and 7.58, respectively [34]. The microscopic environment of DMC was fairly more rigid in BSA nanoparticles as compared to BSA native, which was supported by its higher emission intensity in the nanoparticles form. Interestingly K value obtained by following the changes in fluorescence intensity of DMC was ~ tenfold lower than those estimated by Trp quenching. The fluorescence enhancement of DMC upon binding to BSA native or nanoparticles takes in account of only hrdrophobic interactions. On contrary, the quenching of Trp may be due to combination of both ground state (static) and energy transfer with DMC [35]. Accordingly K value obtained by Trp quenching is expected to have contributions from both

static interaction and the energy transfer. The observed differences in K value can be attributed to above phenomenon. It is also worth to mention that under a condition where the ligand is a fluorescent molecule, it would be ideal to perform the binding studies by monitoring the fluorescence of both protein and ligand separately for the correct representation of binding strength. Finally direct energy transfer between the excited Trp and ground state DMC revealed a close proximity between DMC binding site and Trp residue of BSA native or nanoparticles. On contrary to hydrophobic ligands, if the interaction of ligand or molecule with albumin protein is through ion–dipole and electrostatic interactions, then the fluorescence techniques may not predict the correct strength of binding and in such cases it would be ideal to use absorption techniques [36]. In conclusion, the methodology described in the manuscript is of interest to a wide audience involved in pharmaceutical, food and nutraceutical sectors to study interaction of protein in different physical forms with any hydrophobic ligand.

Funding N/A.

Compliance with Ethical Standards

Conflict of interest The authors declare that they have no conflict of interest.

Informed Consent N/A.

Research Involving Human Participants or Animals This article does not contain any studies with human participants or animals performed by any of the authors.

References

1. Joye IJ, McClements DJ (2016) Curr Top Med Chem 16(9):1026–1039
2. Joye IJ, McClements DJ (2014) Curr Opin Colloid Interface Sci 19(5):417–427
3. Lohcharoenkal W, Wang L, Chen YC, Rojanasakul Y (2014) Biomed Res Int. 2014:Article ID 180549. (https://doi.org/10.1155/2014/180549)
4. Corradini MG, Demol M, Boeve J, Ludescher RD, Joye IJ (2017) Food Biophys 12(2):211–221
5. Kim Y, Ko SM, Nam JM (2016) Asian J Chem 11(13):1869–1877
6. Curry S (2009) Drug Metab Pharmacokinet 24(4):342–357
7. Kratochwil NA, Huber W, Müller F, Kansy M, Gerber PR (2002) Biochem Pharmacol 64(9):1355–1374
8. Roy S (2016) J Pharm Toxicol Stud 4(2):7–17
9. Bronze-Uhle ES, Costa BC, Ximenes VF, Lisboa-Filho PN (2016) Nanotechnol Sci Appl 10:11–21
10. Yu Z, Yu M, Zhang Z, Hong G, Xiong Q (2014) Nanoscale Res Lett 9(1):343–350
11. Miele E, Spinelli PG, Miele E, Tomao F, Tomao S (2009) Int J Nanomed 4(7):99–105
12. Nicolas LF, Chubukov V, Clark LA, Brown S, Teresa HG (2005) Protein Sci 14(4):993–1003
13. Langer K, Balthasar S, Vogel V, Dinauer N, Briesen HV, Schubert D (2003) Int J Pharm 257(1):169–180
14. Das RP, Singh BG, Kunwar A, Ramani MV, Subbaraju GV, Hassan PA, Priyadarsini KI (2017) Colloids Surf B 158:682–688
15. Fanciullino R, Ciccolini J, Milano G (2013) Crit Rev Oncol Hematol 88(3):504–613
16. Yan YI, Marriott G (2003) Curr Opin Chem Biol 7(5):635–640
17. Ghisaidoobe AB, Chung SJ (2014) Int J Mol Sci 15(12):22518–22538
18. Lee MM, Peterson BR (2016) ACS Omega 1(6):1266–1276
19. Kocaadam B, Şanlier N (2017) Crit Rev Food Sci Nutr 57(13):2889–2895
20. Lee WH, Loo CY, Bebawy M, Luk F, Mason RS, Rohanizadeh R (2013) Curr Neuropharmacol 11(4):338–378
21. Barik A, Priyadarsini KI (2013) Spectrochim Acta A 105:267–272
22. Banerjee M, Chakravarty D, Ballal A (2015) BMC Plant Biol 15(16):1–17
23. James NG, Jameson DM (2014) Methods Mol Biol 1076(3):29–42
24. Li CVJ, Wowor AJ (2008) Methods Cell Biol 84(7):243–262
25. Fruhwirth GO, Ameer-Beg S, Cook R, Watson T, Tony N, Festy F (2010) Opt Express 18(11):11148–11158
26. Walsh AJ, Sharick JT, Skala MC, Beier HT (2016) Biomed Opt Express 7(4):1385–1399
27. Vakser IA (2014) Biophys J 107(8):1785–1793
28. Lakowicz JR (1999) Principles of fluorescence spectroscopy, 2nd edn. Kluwer Academic/Plenum Publishers, New York
29. Raut S, Chib R, Butler S, Borejdo J, Gryczynski Z, Gryczynskic I (2014) Methods Appl Fluoresc 2(3):1–8
30. Sahoo B, Balaji J, Nag S, Kaushalya SK, Maiti S (2008) J Chem Phys 129(7):075103
31. Lindgren M, Sörgjerd K, Hammarström P (2005) Biophys J 88(6):4200–4212
32. Bong PH (2000) Bull Korean Chem Soc 21(1):81–86
33. Mariam J, Sivakami S, Dongre PM (2016) Drug Deliv 23(8):2668–2676
34. Shaikh SAM, Singh BG, Barik A, Ramani MV, Balaji NV, Subbaraju GV, Naik DB, Priyadarsini KI (2018) Spectrochim Acta A 199:394–402
35. Shi JH, Pan DQ, Jiang M, Liu TT, Wang Q (2016) J Photochem Photobiol B 164(8):103–111
36. Kastritis PL, Bonvin AMJJ, Soc JR (2013) Interface 10(79):20120835